Draft version September 2, 2020
Preprint typeset using LaTeX style emulateapj v. 12/16/11

THE CLUSTERS HIDING IN PLAIN SIGHT (*CHiPS*) SURVEY: COMPLETE SAMPLE OF EXTREME BCG CLUSTERS

Taweewat Somboonpanyakul[1], Michael McDonald[1], Massimo Gaspari[2,3], Brian Stalder[4,5], and Antony A. Stark[5]

Draft version September 2, 2020

ABSTRACT

We present optical follow-up observations for candidate clusters in the Clusters Hiding in Plain Sight (*CHiPS*) survey, which is designed to find new galaxy clusters with extreme central galaxies that were misidentified as bright isolated sources in the ROSAT All-Sky Survey catalog. We identify 11 cluster candidates around X-ray, radio and mid-IR bright sources, including seven well-known clusters (both starburst-hosting and QSO-hosting), three new candidates which are observed further with *Chandra*, and one candidate that fails secondary inspection. Of the three new candidates, we confirm two newly discovered galaxy clusters: CHIPS1356-3421 and CHIPS1911+4455. The details about CHIPS1356-3421 were presented in our previous publication. The second new cluster, CHIPS1911+4455 at $z = 0.485$, has a total mass $\mathrm{M}_{500} = 6.0\pm0.1\times10^{14}\mathrm{M}_{\odot}$ with a bolometric X-ray luminosity of $L_{\mathrm{x}} = 1.9\times10^{45}$ erg s^{-1}. The cluster is luminous enough to be detected and identified as a cluster in the ROSAT All Sky-Survey data if not because of its bright central core. This newly-discovered cluster is similar in many ways to the Phoenix cluster, but with a highly-disturbed X-ray morphology on large scales. We find the occurrence rate for clusters that would appear to be X-ray bright point sources in any X-ray all-sky surveys to be $2 \pm 1\%$, and the occurrence rate of clusters with runaway cooling in their cores to be $\sim 1\%$, consistent with predictions of Chaotic Cold Accretion. With the number of new groups and clusters predicted to be found with *eROSITA*, the population of clusters that appear to be point sources (due to a central QSO or a dense cool core) could be around 2000. Finally, this survey demonstrates that the Phoenix cluster is likely the strongest cool core at $z < 0.7$ – anything more extreme would have been found in this survey.

Subject headings: galaxies: clusters: general — galaxies: clusters: intracluster medium — X-rays: galaxies: clusters

1. INTRODUCTION

Clusters of galaxies are the largest and most massive gravitationally bound objects in the universe, with masses of roughly $10^{14} - 10^{15} M_{\odot}$ (Voit 2005). Because of their massive scale, these masses have to come from large regions of diameter tens of Mpc. On this scale, the density field remain in the linear regime of density perturbation (Henry & Arnaud 1991). This means that their number densities can be predicted based on first principles, e.g., the Press-Schecter theory (Press & Schechter 1974), which depends strongly on several cosmological parameters, including Ω_m (the density of total matter compare) and σ_8 (the amount of fluctuation in matter density) (Vikhlinin et al. 2009b). This forms the basis of cluster cosmology.

Since the end of the *Planck* Satellite's mission (Planck Collaboration et al. 2018), we are now living in the era of precision cosmology where cosmological parameters of the universe can be measured accurately (to a few percent). To improve the precision of cluster cosmology, various groups have been trying to increase the number of galaxy clusters. There are three main ways to detect galaxy clusters, including overdensities of red galaxies in optical or near-infrared (Gladders & Yee 2000; Rykoff et al. 2014; Gonzalez et al. 2019), extended extragalactic emission in X-ray (Ebeling et al. 2000, 2001; Böhringer et al. 2004), and with Sunyaev-Zel'dovich (SZ) effect (Sunyaev & Zeldovich 1972; Bleem et al. 2015, 2019; Planck Collaboration et al. 2016) in millimeter/sub-millimeter surveys. Each technique has their own unique benefits and challenges. With the invention of wide field optical telescopes, performing optical surveys to find overdensities of galaxies is relatively cheap although optical surveys are strongly affected by projection effects. For SZ surveys, we are capable of detecting galaxy clusters up to relatively high redshift since the SZ signature is redshift independent although we are still limited to only the most massive clusters (Carlstrom et al. 2002; Motl et al. 2005). Lastly, X-ray surveys have been our main technique to detect galaxy clusters since the launch of the ROSAT X-ray satellite (e.g., the REFLEX survey (Böhringer et al. 2004)). Even though X-ray surveys can only produce flux-limited samples of galaxy clusters, cosmologists can take that into account in their selection function when they estimate cosmological parameters (Allen et al. 2008; Vikhlinin et al. 2009b; Mantz et al. 2015).

However, with the recent SZ discovery of the Phoenix

[1] Kavli Institute for Astrophysics and Space Research, Massachusetts Institute of Technology, 77 Massachusetts Avenue, Cambridge, MA 02139
[2] Department of Astrophysical Sciences, Princeton University, Princeton, NJ 08544, USA
[3] INAF, Osservatorio di Astrofisica e Scienza dello Spazio, via Piero Gobetti 93/3, 40129 Bologna, Italy
[4] Vera C. Rubin Observatory Project Office, 950 N. Cherry Ave, Tucson, AZ 85719, USA
[5] Center for Astrophysics — Harvard & Smithsonian, 60 Garden Street, Cambridge, MA 02138, USA

cluster (McDonald et al. 2012, 2015), the most X-ray luminous galaxy cluster known, at $z = 0.6$, we start to question our understanding of the X-ray-survey selection function. The Phoenix cluster was detected in several previous X-ray surveys, but was misidentified as a bright point source based on its extremely bright active galactic nucleus (AGN) and cool core in the center of the cluster. With most X-ray surveys identifying objects as either a point-like or an extended source, a galaxy cluster with a bright point source in the center would be misidentified as simply a point source. The next logical step is to ask how many of these galaxy clusters we have missed in the previous surveys, and how this translates to a correction for the selection function.

Another benefit of finding galaxy clusters hosting bright X-ray point sources is related to the cooling flow problem, which is the lack of newborn stars in a cluster core even though the hot intracluster medium (ICM) is cooling intensely through its X-ray emission. The best candidate for explaining the inconsistency is AGN feedback from the central galaxy (Bower et al. 2006; Croton et al. 2006; Bower et al. 2008). There are two main modes of AGN feedback: the kinetic mode, driven mostly by jets, and the radiative mode, driven by the accretion of the AGN (Fabian 2012; McNamara & Nulsen 2012; Harrison 2017; Gaspari et al. 2020). With very few known galaxy clusters with extremely bright quasars, such as H1821+643 (Russell et al. 2010), 3C 186 (Siemiginowska et al. 2005, 2010), 3C 254 (Crawford & Fabian 2003; Yang et al. 2018), IRAS09104+4109 (O'Sullivan et al. 2012), and the Phoenix cluster (McDonald et al. 2012), a larger number of such objects are required to fully understand the role of radiative-mode feedback in the evolution and formation of galaxy clusters. For example, Chaotic Cold Accretion (CCA) model predicts a tight co-evolution between the central supermassive black hole (SMBH) and the host cluster halo (via the cooling rate or $L_{\rm x}$; Gaspari et al. 2019), with flickering quasar-like peaks reached only a few percent of times (Gaspari et al. 2017).

In an attempt to find more galaxy clusters hosting bright central point sources, we started the Clusters Hiding in Plain Sight (*CHiPS*) survey. The details and the first discovery from the survey is published in Somboonpanyakul et al. (2018). In this paper, we focus on a new optical cluster finding algorithm, developed specifically for the *CHiPS* survey, to look for cluster candidates after optically imaging all of the X-ray point sources with bright radio and mid-IR from the first part of the project. These candidates may have been misidentified in previous all-sky surveys due to their central galaxies' brightness. After performing the cluster finding algorithm, we present a list of newly-discovered galaxy cluster candidates along with their expected redshift and richness.

The overview of the *CHiPS* survey, the optical data used in the follow-up campaign, and its methodology are described in Section 2. In Section 3, we present details of the data reduction and analysis for recently-obtained optical data from the Magellan telescope. Our cluster finding algorithm is described in Section 4 while the X-ray data reduction is presented in Section 5. We discuss the results and the implications of this finding in Section 6 and 7. Lastly, we summarize the paper in Section 8. We assume $H_0 = 70\,\mathrm{km\,s^{-1}\,Mpc^{-1}}$, $\Omega_\mathrm{m} = 0.3$ and $\Omega_\lambda = 0.7$. All errors are 1σ unless noted otherwise.

2. THE *CHIPS* SURVEY

The *CHiPS* survey is designed to identify new centrally concentrated galaxy clusters and clusters hosting extreme central galaxies (starbursts and/or AGNs) within the redshift between 0.15 and 0.7. The first part of the survey consists of finding candidates from combining several all-sky survey catalogs to look for bright objects in multiple wavelengths. The second part of the survey, which is the focus of this paper, addresses mainly our optical follow-up program to determine the best cluster candidates by finding an overdensity of galaxies with similar redshifts centered on the location of the X-ray sources. The last part, which is also included in this paper, is to obtain *Chandra* data for these candidates in order to confirm the existence of these new clusters and characterize their properties, such as the gas temperature, the total mass, and the gas fraction.

2.1. *Target Selection*

Our *CHiPS* target selection is described in detailed in our previous publication (Somboonpanyakul et al. 2018); here we outline the main steps.

To select systems similar to the Phoenix cluster, we require sources to be bright in X-ray, mid-IR and radio, relative to near-IR. The normalization to near-IR is to prevent nearby low-luminosity sources from overwhelming the sample. Starting with X-ray point source catalogs from the *ROSAT* All-Sky Survey Bright Source Catalog and Faint Source Catalog (RASS-BSC and RASS-FSC; Voges et al. 1999), we cross-correlate it with radio from NVSS (Condon et al. 1998) or SUMSS (Mauch et al. 2003), mid-IR with WISE (Wright et al. 2010), and near-IR with 2MASS (Skrutskie et al. 2006). This combination leads to two types of astrophysical sources: radio-loud type II QSOs and galaxy clusters with an active core (a starburst and/or AGN-hosting BCG). This approach is similar to two other surveys from Green et al. (2017) and Donahue et al. (2020). The main difference is that Donahue et al. (2020) focus on previously-known optically-selected BCG from the GMBCG catalog (Hao et al. 2010) and Green et al. (2017) started with spectroscopically confirmed AGN in the ROSAT catalog. We begin our search with a complete ROSAT point source catalog and combine with all archival data from near-IR, mid-IR to radio.

In addition, we apply color cuts in order to select only the most extreme objects in X-ray, mid-IR, and radio, as demonstrated in Fig 1. The cuts are chosen to capture the expected range of color for a Phoenix-like object at an unknown redshift between 01 and 0.7. The NASA/IPAC Extragalactic Database (NED)[6] was used to reject foreground ($z < 0.15$) and background ($z > 0.7$) objects. Candidates with $z < 0.15$ are close enough to be detected with past instruments even with a bright central point source. Most of these clusters were first detected by eye in various optical catalogs, including the well-known Abell and Zwicky catalogs, which means that we do not expect any misclassifications. On the other hand, objects with $z > 0.7$ are exceedingly challenging to detect an overdensity of red galaxies, using ground-based telescopes. We also remove objects which have galactic

[6] https://ned.ipac.caltech.edu

latitude less than $\pm 15^\circ$ because foreground stars and extinction from the Milky Way will obscure any clusters. After the removal, we are left with 470 objects to perform the optical follow-up, which is presented in the upcoming section.

Further information about our target selection and the first galaxy cluster discovered from this survey, the galaxy cluster surrounding PKS1353-341, are presented in Somboonpanyakul et al. (2018). In the next section, we describe all the data used for the optical follow-up to look for an overdensity of red galaxies, which is a signature of a galaxy cluster.

2.2. *Optical Follow-up Observations*

The optical follow-up program is separated into two parts based on the declination of the targets. Most objects with positive declination are followed up with the Sloan Digital Sky Survey (SDSS) because of its nearly complete coverage in the Northern Sky. Whereas, objects with negative declination are observed with either the first data release of the Panoramic Survey Telescope and Rapid Response System (Pan-STARRS1; Chambers et al. 2016) with sky coverage of declination greater than -30° or additional pointed observations using the Parallel Imager for Southern Cosmological Observations (PISCO; Stalder et al. 2014) on the 6.5m Magellan Telescope at Las Campanas Observatory, Chile. Specifically, 256 out of our 470 candidates were observed with SDSS, 64 candidates were observed with Pan-STARRS1, and the remaining 150 candidates were individually observed with PISCO on the Magellan telescope. We note that data from the Dark Energy Survey (DES; Dark Energy Survey Collaboration et al. 2016) was unavailable at the onset of the project. Fig. 2 shows the position of all target candidates in the sky, separated by the telescope used for the follow-up.

2.2.1. *Sloan Digital Sky Survey (SDSS)*

The Sloan Digital Sky Survey (SDSS) is a multi-spectral imaging and spectroscopic redshift survey using a 2.5-m optical telescope at Apache Point Observatory in New Mexico (Gunn et al. 2006). We utilized Data release 14 (DR14), released in 2017, which is the second data release for SDSS-IV (Abolfathi et al. 2018). We retrieved the photometric data in u, g, r, i, and z bands by querying objects within a radius of 5 arcmin from the X-ray position, using the function `fGetNearestObjEq` with the Casjob server[7]. In Section 4, we apply a more stringent cut during the cluster finding algorithm. We obtained the SDSS model magnitude (`modelMag`), as explained in the SDSS support documentation[8] that the model magnitudes give the most unbiased estimates of galaxy colors. To convert SDDSS magnitude to flux units, we use the SDSS asinh magnitude formula[8], which is also described in (Lupton et al. 1999).

For star/galaxy classification, "`type`" parameters, provided by SDSS, were used to select only galaxies (`type` = 3). The classification is based on the difference between cmodel and PSF magnitude. Specifically, an object is classified as extended when $\mathrm{Mag_{PSF}} - \mathrm{Mag_{cmodel}} > 0.145$. In addition, we downloaded photometric redshifts (z_{sdss}) for photometric redshift estimate verification in Section 4.

[7] https://skyserver.sdss.org/CasJobs/

[8] https://www.sdss.org/dr12/algorithms/magnitudes/

2.2.2. *Panoramic Survey Telescope and Rapid Response System (Pan-STARRS)*

Pan-STARRS is a system for wide-field astronomical imaging in the optical g, r, i, z, and y bands, located at Haleakala Observatory, Hawaii. The survey used a 1.8-m telescope, with an imaging resolution of $0.25''$/pixel from its 1.4 Gigapixel camera. Pan-STARRS1 (PS1), the basis for Data release 1 (DR1), covers three quarters of the sky (3π survey) north of a Declination of -30°.

Star/galaxy separation of PS1 is similar to that of SDSS. Specifically, the difference between model and PSF magnitude is measured to identify extended objects. However, instead of applying a simple straight line as a cut (e.g., $\mathrm{Mag_{PSF}} - \mathrm{Mag_{Kron}} > 0.05$ where $\mathrm{Mag_{Kron}}$ is Kron magnitudes as the representation for model magnitude), an exponential model is used to fit the bright part of Fig. 3 and then extrapolated to fainter objects, similar to (Chambers et al. 2016). More details discussion about this technique can be found in (Farrow et al. 2014). As shown in Fig. 3, the star-galaxy separation is not a horizontal cut, but an exponential curve which takes into account our inability to distinguish between stars and galaxies at the fainter end. We require the cut to be satisfied for both r and i band. Even though this star-galaxy-separation criterion could identify more objects as galaxies, this should not create a large bias for our cluster-finding algorithm. We chose Kron magnitudes as the Pan-STARRS magnitudes for our algorithm since they capture more light from the extended parts of galaxies, compared to PSF magnitudes.

2.2.3. *Magellan Telescope with PISCO*

Without a more robust all-sky survey in the southern sky similar to SDSS and Pan-STARRS in the north, we perform 150 individual follow-up observations for targets in the southern sky with the 6.5-m Magellan telescope. PISCO, a multi-band photometer, is used to speed up our observations because of our large number of candidates. With the ability to produce g, r, i, and z band images simultaneously, our effective efficiency in observing these candidates increases by a factor of ~ 3 (including optical losses; Stalder et al. 2014). All candidates were acquired with PISCO during 9 nights splitting over 3 observing runs between 2017 January to 2017 December. We observed most objects with 5-minute total exposure with two 2.5-minute exposures for dithering. To analyze the PISCO data, we have created a data processing pipeline. More details about data reduction and star/galaxy separation for *CHiPS* is presented in the next section.

2.3. *X-ray Follow-up Observations*

To confirm the existence of a galaxy cluster, we require an X-ray observation, specifically showing extended emission, indicating an extremely hot intracluster medium (ICM), which is expected for the deep potential well of a cluster. The *Chandra* X-ray Observatory is best suited for the task, given that our targets may have bright central point sources. With an angular resolution of 0.5 arcsecond, *Chandra* has the capability to distinguish X-ray point sources (e.g., AGN) from the extended

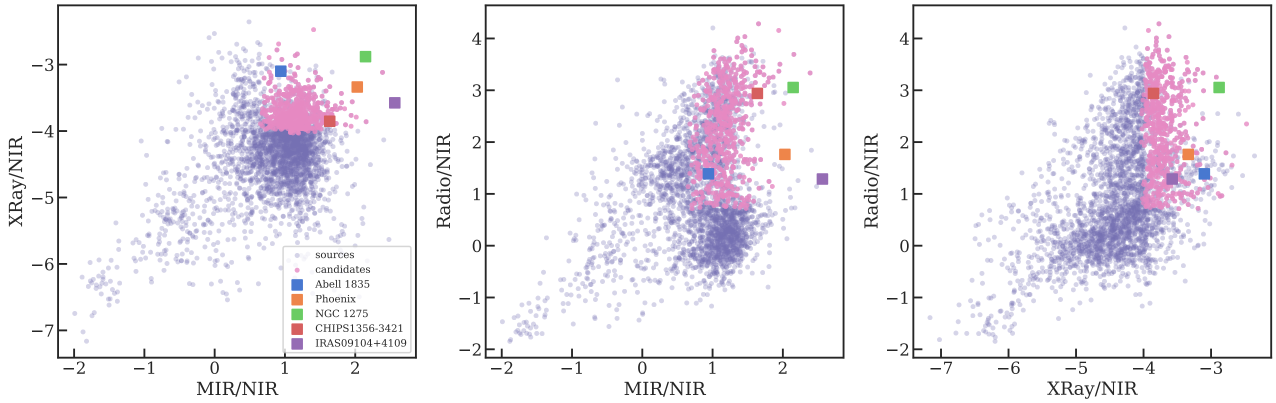

FIG. 1.— The three panels show color-color diagrams for objects that are detected in all four all-sky surveys (3,450 objects). The axes are the logarithm of the ratio of the X-Ray, mid-IR (MIR) or radio flux to the near-IR (NIR) flux. Points colored in pink satisfy our three color cuts. The Phoenix, Perseus (NGC 1275), Abell 1835, and IRAS09104+4109 clusters, which host extreme BCGs, are shown with orange, green, blue and purple squares, respectively while CHIPS1356-3421 is shown with a red square.

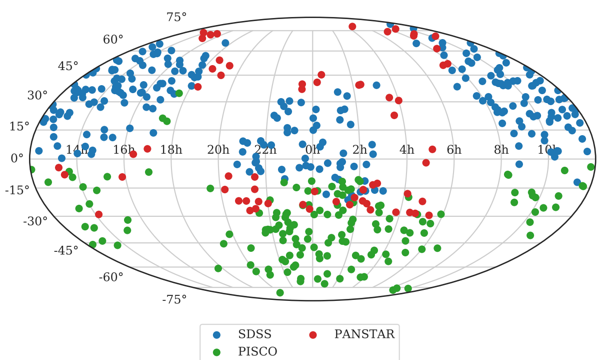

FIG. 2.— Plot of all 470 target candidates for the *CHiPS* survey in the sky. The blue dots represented candidates followed-up with SDSS. The red dots are candidates followed-up with Pan-STARRS, and the green dots are candidates from PISCO observations. The gaps at RA = 18h-20h and 5h-7h corresponds to the Milky Way which prevents us from finding new cluster candidates around that region.

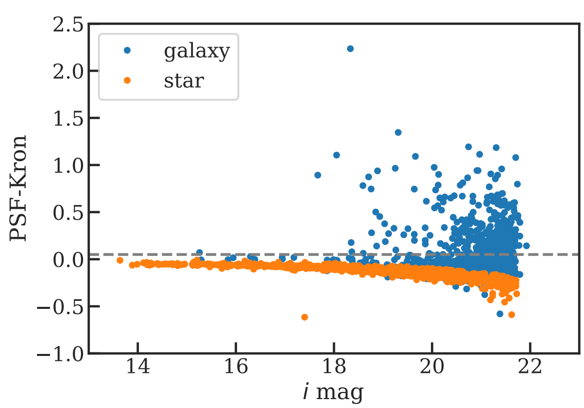

FIG. 3.— This figure demonstrates how we separate stars and galaxies in the Pan-STARRS sample catalog using the ratio of PSF and Kron magnitudes. The orange color indicates stars, which pass both the r and i band cut while the blue color marks galaxies.

emission of the ICM. We observed a total of 4 additional candidates from the CHIPS survey, apart from the initial sample of 4 candidates for the pilot study (Somboonpanyakul et al. 2018). More details about the reduction process for the X-ray data can be found in Section 5.

3. PISCO OBSERVATIONS AND DATA PROCESSING

In this section, we describe the data reduction process for the PISCO data. Since we obtain raw images from the PISCO instrument on the Magellan telescope, we developed a complete reduction pipeline to convert these images to photometry for all galaxies in the field, which is then used as an input for our cluster finding algorithm. In contrast, SDSS and Pan-STARRS are complete all-sky surveys with available photometric catalogs, which do not require any further data processing.

3.1. *PISCO Image Reduction*

PISCO is a photometer that produces g, r, i, and z band images simultaneously (Stalder et al. 2014). The camera is composed of four 3k×4k charge-coupled devices (CCDs), one for each of the four focal planes, with an un-binned scale of $0.109''$ per pixel, resulting in a $5' \times 9'$ field of view. Each CCD is read out with two amplifiers.

For each image, the data reduction process consists of several steps as follows. First, the median of all bias frames for each night is subtracted from both the median of all flat frames and the science frames. We do not subtract the dark currents since they are negligible in these devices. The ratio between the two subtracted frames (flat and science) is the flat-fielded image. The two flat-fielded images from the two amplifiers of a CCD are stitched together to create a complete image for each band (g, r, i, and z) and each exposure. L.A. Cosmic is run on each image for robust cosmic rays detection and removal (van Dokkum 2001) to reduce the number of confusion sources when we perform astrometry. Then, the astrometry is carried out via Astrometry.net[9], which is used to find the pointing, scale, orientation, and rough astrometric calibration of each image (Lang et al. 2010).

Each photometric band and exposure need to be coadded to create a final image with the right alignment for

[9] http://astrometry.net

each band. First, an initial source detection is run on all science images using `SExtractor` (Bertin & Arnouts 1996). Objects which are corrupted or truncated are removed from the lists by requiring the `FLAGS` parameter to be less than 5. Next, `SCAMP` (Bertin et al. 2002) is run over all of the images simultaneously to improve the astrometric solutions, previously obtained from Astrometry.net. The reference catalog we used for the astrometry is linked to the Two Micron All Sky Survey (2MASS) catalog (Skrutskie et al. 2006). The individual images of each band are then resampled and coadded via `SWarp` (Bertin 2006). An example of the final processed image is shown in Fig. 4.

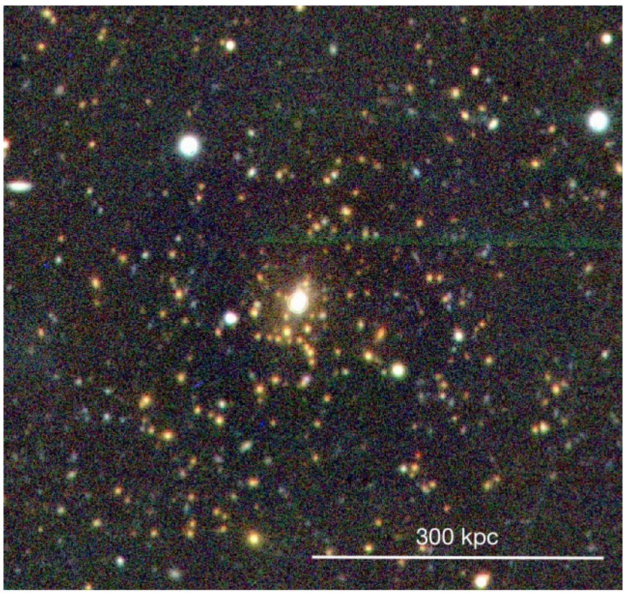

Fig. 4.— The RGB image of the Phoenix cluster from PISCO with g, r, and i bands. The image shows several red galaxies centrally located in the field, which is the signature of a galaxy cluster. The extremely bright point source in the center is a reason why the Phoenix cluster had been missed from previous X-ray surveys.

3.2. *Seeing Estimation and PSF Models*

Even though each image already has an estimated seeing, a more precise value is required. We achieve this by fitting the Point Spread Function (PSF) models to every object in the field and picking the most common PSF to represent the seeing of that particular field. Specifically, the first step is creating 45×45-pixel small subimage ("vignette") for each detected object by using `SExtractor`. These small vignettes are fitted with the 2D-Moffat model, available in the Astropy model packages (Astropy Collaboration et al. 2018). The Moffat model is a probability distribution that more accurately represents PSFs whose wings cannot be portrayed by a simple 2D-Gaussian function. In this case, a seeing means the full width at half maximum (FWHM) of the fitted model. Fig. 5 shows the seeing distribution for all 262 fields observed with the PISCO camera. The median seeing in g, r, i, and z bands are $1.''15$, $1.''19$, $1.''04$, and $0.''99$ respectively, meaning that the seeings tend to be larger for bluer bands as we expect. The seeing distributions are not symmetric, but highly skewed toward higher seeing, representing a variation in the weather at the time of observation.

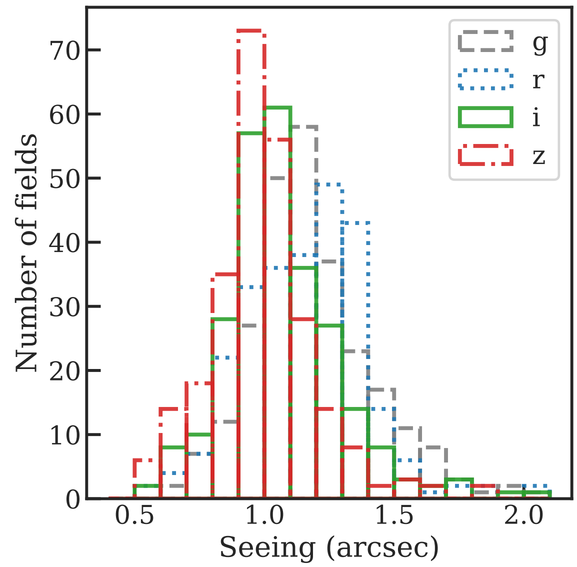

Fig. 5.— Seeing distribution for the 262 fields observed with PISCO. The g band is traced by black dashed lines, the r band is traced by blue dotted lines, the i band is traced by green solid lines, and the z band is traced by red dot-dashed lines. The median values of the seeing in g, r, i, z bands are $1.''15$, $1.''19$, $1.''04$, $0.''99$ respectively.

Apart from an accurate seeing estimate, the PSF model is also required for `SExtractor` to measure MAG_PSF. `PSFEx` is a software used to extract the PSF models from FITS images (Bertin 2011). All parameters in `PSFEx` are set to default. To get a good model for the PSF, we need to only select well-behaved point sources (stars) as our model. We achieve this by selecting sources which are not at the edges of the CCD, not elongated, and have a typical effective flux radius (within 2σ from the mean of all radii in the field).

3.3. *Source Extraction*

To measure an accurate color for each object, we extracted photometry via the dual-image mode of `SExtractor`, which uses the same pixel location for all photometric bands. The seeing estimates and the PSF models are used in this step with other input parameter described in Table 1. Next, we extract *griz* MAG_AUTO, MAG_APER, and MAG_PSF at the location of detected sources from the i-band image.

3.4. *Star-Galaxy Seperation*

One of the most important steps for the reduction pipeline is to separate sources into stars and galaxies. While CLASS_STAR[10] is often used for this purpose, upon our close investigation we found non-negligible amount of confusions in both star and galaxy samples. Instead, we use the SPREAD_MODEL parameter which indicates whether a local PSF model or a more extended

[10] https : //sextractor.readthedocs.io/en/latest/ClassStar.html

TABLE 1
SExtractor Source Detection Input Parameters

Parameter	Value
DETECT_MINAREA	$1.1\pi \times (i\,\text{band seeing}^2)$
DETECT_THRESH	1.2
GAIN	0.25
PIXEL_SCALE[a]	0.12 or 0.22
SATUR_LEVEL	61,000

[a] Depending on whether the data is binned.

model better match the source (Mohr et al. 2012). It is defined to be the difference between convolving a galaxy model with the image and with a local PSF model. By design, SPREAD_MODEL is close to zero for point sources and positive for extended sources. This estimator has been used in several surveys, e.g., the Blanco Cosmology Survey (BCS) (Desai et al. 2012) and the Dynamical Analysis of Nearby Cluster (DANCe) survey (Bouy et al. 2013). In particular, we separate stars and galaxies by the following criteria:

$$\begin{aligned} galaxies &: \text{SPREAD\_MODEL\_I} > 0.005 \\ &\quad \& \, \text{MAG\_i} < 17.5 \\ stars &: \text{SPREAD\_MODEL\_I} < 0.004, \end{aligned} \tag{1}$$

where MAG_i is the magnitude of the object in i band. This criteria is adapted from Sevilla-Noarbe et al. (2018), providing a better separation between stars and galaxies, compared to CLASS_STAR, because we take into account the PSF variation in the calculation. The exact values of the thresholds are not exceedingly crucial since we will later estimate the photometric redshfits (z_{phot}) for each object, as shown in Section 4.1. If an object is wrongly identified as a galaxy, we will not obtain a good fit for z_{phot} and the object will be removed from the cluster finding algorithm. More details and different tests to quantify the performance of this star-galaxy statistic can be found in Sevilla-Noarbe et al. (2018).

3.5. *Photometric Calibration*

To calibrate the color and the magnitudes of stars and galaxies, we use Stellar Locus Regression (SLR; High et al. 2009). SLR adjusts the instrumental colors of stars and galaxies and simultaneously solves for all unknown zero-points by matching them to a universal stellar color-color locus and the known 2MASS catalog. The calibration takes into account difference in instrumental response, atmospheric transparency, and galactic extinction. SLR has been used to calibrate the photometry in the literature for various surveys including SPT-detected galaxy clusters follow-up (High et al. 2010) and Blanco Cosmology Survey (BCS; Bleem et al. 2015). The specific implementation of the algorithm we utilize here is described in Kelly et al. (2014).

For each frame, we use the stellar sources identified in Section 3.4 as the starting point. We then perform the stellar locus regression, simultaneously solve for all the unknown zeropoints, and convert the magnitudes extracted from SExtractor to the SDSS system using a single set of corrections. Whereas, the absolute flux scaling is calibrated with SLR using the 2MASS point source catalog (Skrutskie et al. 2006).

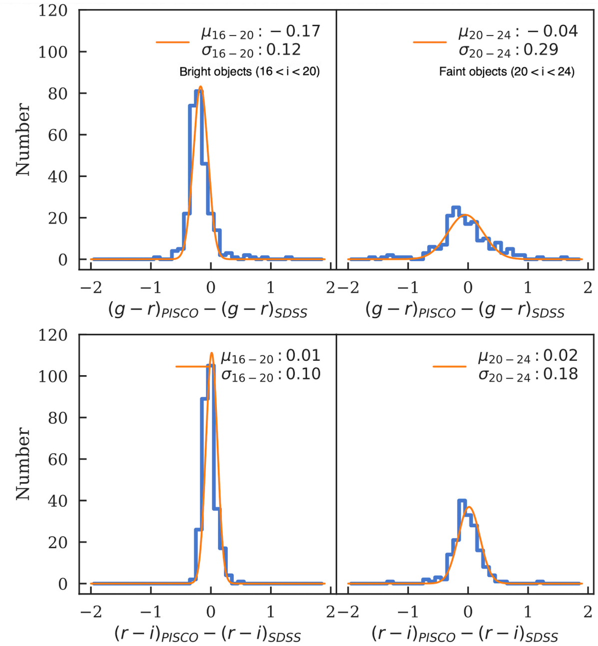

Fig. 6.— The top two panels show a comparison of $g-r$ between PISCO PSF magnitude and SDSS PSF magnitude while the bottom two show a comparison of $r-i$. The left panels corresponds to bright objects ($16 < i_{\rm PISCO} < 20$) while the right panels corresponds to fainter ones ($20 < i_{\rm PISCO} < 24$). The orange lines are the gaussian best-fit model with its mean and its standard deviation in the legend. This demonstrate that for bright objects, the scatter of the PISCO calibration from the SDSS is about 0.10-0.12 mag, which is similar to that of Pan-STARRS, as shown in Fig. 7.

3.6. *Photometric Verification*

We perform a comparison test to check the accuracy of the photometric calibration. The test is carried out by comparing between the colors ($g-r$, and $r-i$) we obtained from the PISCO pipeline and the SDSS colors. We observed three fields in our SDSS target list (SDSS123, SDSS501, SDSS603) with PISCO, and reduced the data using the same PISCO pipeline we developed in this section. Galaxies found in the SDSS catalog are matched with objects in our observed PISCO frames based on their celestial coordinates. The objects are plotted in Fig. 6, showing the offsets between the color from PISCO and SDSS. The offsets are related to different filters used in the three telescopes. The scatter of the PISCO colors compared to the SDSS colors is around 0.12 mag, which is similar to the scatter we found from comparing the Pan-STARRS colors to the SDSS colors, as shown in Fig. 7. This shows us that our color calibration for PISCO is as accurate as the calibration between SDSS and Pan-STARRS.

4. CLUSTER FINDING ALGORITHM

In this section, we describe the new cluster finding algorithm. Because of the nature of our survey, which looks for cluster candidates surrounding X-ray sources, we already have the central location of the cluster, which we assume to be the location of the X-ray sources. This means that unlike other optical cluster finding surveys, we do not use a friend-of-friend algorithm (Huchra & Geller 1982) to search for the center of the cluster. In-

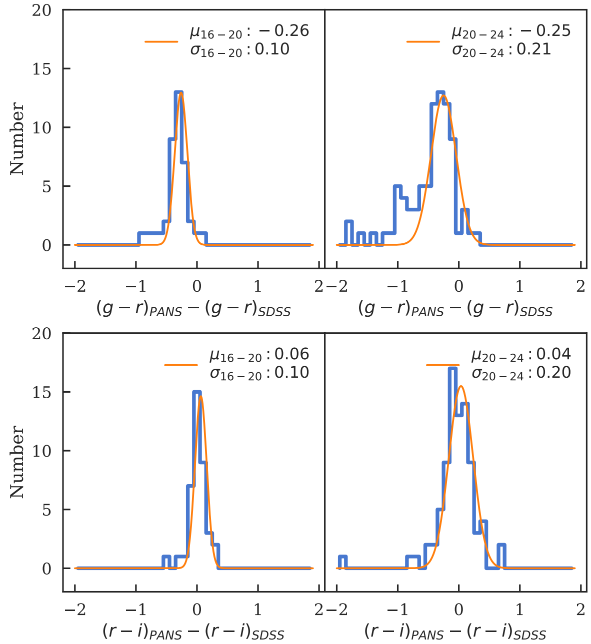

Fig. 7.— Same as Fig. 6, except for comparison between Pan-STARRS PFS magnitude and SDSS PSF magnitude. The scatter of Pan-STARRS colors compared to SDSS is 0.10 mag.

stead, we look for an overdensity of galaxies with similar redshifts at the location of the X-ray source.

Specifically, we search for a peak in the redshift histogram of all the galaxies within the observed fields. Members of a galaxy cluster will have similar redshifts, meaning that finding the peak in the redshift histogram will differentiate between cluster members and field galaxies. The peak location corresponds to the redshift of the galaxy cluster.

The algorithm is divided into three parts: photometric redshift measurement, aperture selection and background subtraction, and richness correction for highsredshift clusters.

4.1. *Photometric Redshift*

The first step of the algorithm is to estimate photometric redshifts of all galaxies in the field. Mid-IR data is included in this step to improve constraints. The sections below describes data acquisition for Mid-IR bands from the Wide-field Infrared Survey Explorer (Wright et al. 2010, *WISE*), and the software used for photometric redshift estimates.

4.1.1. *Wide-field Infrared Survey Explorer (WISE)*

WISE is an IR satellite with four IR filters, including $W1$ (3.6 μm), $W2$ (4.3 μm), $W3$ (12 μm), and $W4$ (22 μm). We select galaxies in the AllWISE Source Catalog, using IRSA's Simple Cone Search (SCS)[11], and match them with their optical counterparts from SDSS, Pan-STARRS, or PISCO within a radius of 3". However because the FWHM for $W1$ and $W2$ is rather large ($\sim$ 6", compared to $\sim$ 1" for optical data[12]), we cannot separate different optical galaxies from the *WISE* sources, especially at the center of the cluster where large number of objects are presented in a small region. Thus, we only use the *WISE* measurement from both $W1$ and $W2$ as upper limits to help constrain the photometric redshifts.

4.1.2. *Photometric Redshift Estimate*

Each galaxy's photometric redshift (z_{phot}) is determined by fitting the photometry in optical and Mid-IR bands to the template spectral energy distribution (SEDs) using the Bayesian Photometric Redshifts (BPZ) code (Benítez 2000; Coe et al. 2006). The BPZ code uses Bayesian inference and priors to estimate photometric redshifts using multi-wavelength broad-band data. We used the default templates, consisting of one early-type, two late-type and one irregular-type templates from Coleman et al. (1980) and two starburst templates from Kinney et al. (1996). We also added WISE filters for $W1$ and $W2$ band. Since there is no response filter for the PISCO optical bands, we convert the photometry from PISCO to SDSS bands and use SDSS response filters instead. We do not expect the difference in the response filter to have a large impact on the final redshift since PISCO filters are designed to be as similar to the SDSS filterss as possible.

4.1.3. *Redshift Verification*

To verify our photometric redshifts, we compare 538 redshifts from the BPZ algorithm to those publicly available from SDSS3 (Abolfathi et al. 2018). Typical uncertainties on our redshifts from the BPZ code are $\sigma_z/(1+z) \sim 0.1$, with uncertainties increasing towards higher redshift. In Fig. 8, we show the comparison of BPZ redshifts to those from SDSS3, finding the relative scatter to be $\sim$5%, or less than the typical redshift uncertainty. The median offset between BPZ and SDSS3 redshifts is $\sim$0.03, which is also less than our typical per-galaxy photometric redshift uncertainty. Given this overall agreement, we proceed with BPZ redshifts for the full sample.

4.2. *Aperture Selection and Redshift Histogram*

In terms of aperture selection, we choose a simple top hat model with a radius of one arcminute. This allows us to do a more simple correction for the richness value, as discussed in Section 4.3. Next, we create a histogram representing the redshift distribution of all the galaxies in the selected aperture. Since the peak of a histogram is strongly related to the background level of field galaxies, we estimate the background distribution by making a redshift histogram of field galaxies in all images of each instrument (SDSS, Pan-STARRS, and PISCO). There are $\sim$22,000 background galaxies for PAN-STARR and PISCO, and $\sim$27,000 galaxies for SDSS. We normalized the background histogram for each observation by scaling the total number of objects in the background histogram to be the same as the histogram of interest and subtract from it. The top panel of Fig. 9 shows both the redshift distribution of all the galaxies (in blue) and the normalized distribution of background galaxies (in orange).

The background-subtracted histogram is then used to search for a redshift peak, as shown in the bottom panel of Fig. 9. Since the redshifts estimated from the BPZ

[11] https://irsa.ipac.caltech.edu/docs/vo_scs.html
[12] http://wise2.ipac.caltech.edu/docs/release/allsky/expsup/sec4_4c.html

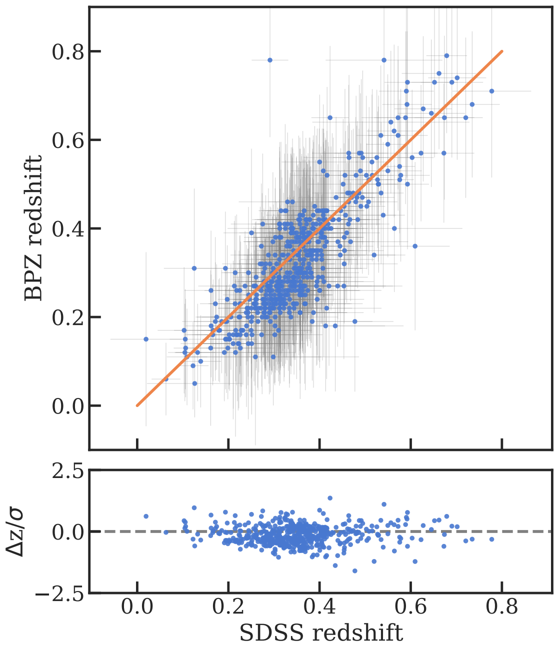

FIG. 8.— Comparison scatter plot between the BPZ redshift and the photometric redshifts from SDSS3. Most of the objects are in an agreement between the two with the relative scatter to be ∼5%.

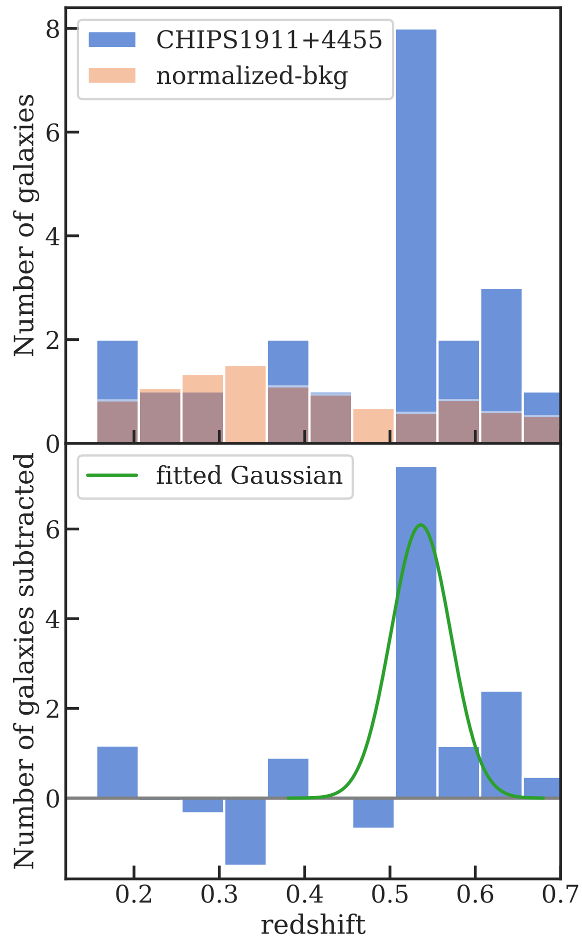

FIG. 9.— Top: The blue histogram shows the redshift distribution of all the galaxies within one arcmin field of view for CHIPS1911+4455. Whereas, the orange histogram shows the the normalized distribution of the background galaxies. Bottom: The background-subtracted histogram is shown in blue. The green solid line shows the fixed-width Gaussian fit between the peak and the two neighboring bins to estimate the richness. The peak of the redshift distribution at $z = 0.53$ implies that we see an overdensity of galaxies, strongly suggesting a galaxy cluster candidate.

code have some uncertainty, we fit a fixed-width Gaussian to the peak and the two neighboring bins to get an estimate for the richness (the amplitude of the Gaussian) and the final redshift (the location of the Gaussian).

4.3. *Richness Correction*

Because observations were made from different optical telescopes and galaxy clusters are located at different redshifts, the richness correction is necessary to have a uniform richness measurement across all fields and all redshifts. The two effects we have taken into account include the luminosity function of galaxies and the evolving angular size of galaxy clusters on the sky. We check both effects and find that the luminosity function correction is larger than the angular diameter correction by a factor of ∼50–1000, depending on the redshift, so we only consider the luminosity correction.

Extremely bright objects tend to be rare, compared to fainter objects, implying that cluster candidates at higher redshift will have fewer observable members since the majority of them will be too faint to detect with our current instruments. This correction is used to remedy the galaxy counts to account for galaxies which are below detection limits. The luminosity function we used comes from Wen & Han (2015) which combines the Schechter function ($\phi_s(M)$) (Schechter 1976) and the composite luminosity function of the BCGs ($\phi_g(M)$):

$$\begin{aligned}\phi_s(M)+\phi_g(M) = 0.4\ln(10)\phi_* 10^{-0.4(M-M_*)(\alpha+1)} \\ \exp\left[-10^{-0.4(M-M_*)}\right] \\ + \frac{\phi_0}{\sqrt{2\pi\sigma}}\exp\left[-\frac{(M-M_0)^2}{2\sigma^2}\right]dM,\end{aligned}$$

where α is the faint-end slope, M_* and M_0 are the characteristic absolute magnitudes, ϕ_* and ϕ_0 are the normalization factors. Another effect related to the luminosity function comes from variability in the depth of the survey in different field/telescopes. Specifically, SDSS is deeper (fainter limiting magnitude) than Pan-STARRS. Whereas, PISCO has a large variation within itself, which comes from the variation in the weather condition when we observed these objects.

Fig. 10 illustrates the richness correction at different redshifts and limiting magnitude (M_{lim}). The correction is strongest when we consider high redshift objects with low limiting magnitude.

4.4. *Flux-Limited Nature of Previous Surveys*

The *CHiPS* survey is designed to look for misidentified galaxy clusters in surveys based on data from the ROSAT telescope. One such survey, the ROSAT-ESO Flux-Limited X-ray (REFLEX) Galaxy Cluster Survey (Böhringer et al. 2004), contains 447 galaxy clusters above an X-ray flux of $\sim 3\times10^{37}\,\mathrm{erg\,s^{-1}\,Mpc^{-2}}$ (0.1-2.4 keV) which are all spectroscopically confirmed.

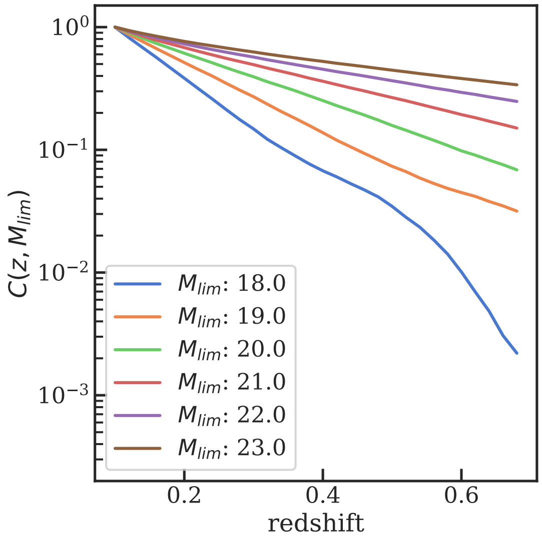

FIG. 10.— Richness correction as a function of redshift and limiting magnitude (M_{lim}) due to the luminosity function of galaxies where there are fewer bright massive galaxies, compared to faint smaller ones. Specifically, $R_{true} = \frac{R_{obs}}{C(z,M_{lim})}$, where $R_{true/obs}$ is the corrected and measured richness, and $C(z, M_{lim})$ is the richness correction.

The left panel of Fig. 11 shows all 447 clusters in the REFLEX sample on an X-ray luminosity ($L_{\rm x}$) vs redshift plot, with the blue line showing the constant flux limit of the REFLEX sample. It is assumed that this survey has found all of the galaxy clusters with luminosities above this limit.

However, some of the X-ray bright point sources detected by ROSAT are believed to be misidentified massive clusters with extreme central galaxies. We want to find clusters exceeding the REFLEX flux limit but still classified as point sources. Since obtaining new optical data is more straightforward to obtain compared to X-ray, we convert this REFLEX flux limit to optical richness limit which can then be used for our richness cut, as described in Section 6.

In order to convert this flux limit to the richness limit, the optical richness of this sample is required. First, we cross-correlate between the REFLEX clusters and SDSS and find 82 clusters that have the SDSS photometry data. By running the same cluster finding algorithm as described in this section, we estimate the richness of all 82 REFLEX clusters. Since both the richness and X-ray luminosity are correlated with the total mass of the clusters, we fit a straight line to the log-log plot, as shown in the middle panel of Fig. 11, to find the relation between the flux limit and the richness limit. The last panel of Fig. 11 shows the richness limit on the richness-redshift plot. All clusters above this line should have been discovered by the REFLEX survey. This implies that any clusters we find from the *CHiPS* Survey which are above this line are either known clusters or misidentified clusters from their bright X-ray point sources.

5. X-RAY DATA REDUCTION

In addition to the optical survey, we perform X-ray follow-up of all promising candidates with *Chandra* in order to look for an extended hot ICM, confirming the existence of a massive cluster. In this section, we describe the X-ray data reduction process to estimate the total mass and luminosity of these clusters. A more detailed analysis with these data is described in (Somboonpanyakul et al. 2018).

All *CHiPS* candidates were observed with *Chandra* ACIS-I for 30-40 ks each. The data was analyzed with CIAO (Fruscione et al. 2006) version 4.11 and CALDB version 4.8.5, provided by Chandra X-ray Center (CXC). The event data was re-calibrated with VFAINT mode, and point sources, which are not in the center, were excluded with the *wavdetect* function. The image was produced by applying *csmooth*, which adaptively smoothed an image with maximal smoothing scale of 15 pixels and signal-to-noise ratio between 2.5 and 3.5.

High angular resolution X-ray images can be used to estimate different properties of the cluster, including the mass and total luminosity. We choose M_{500}, the total mass within R_{500}, the radius within which the average enclosed density is 500 times the critical density ($\rho_c = 3H_0^2/8\pi G$), to represent the total cluster mass. We use scaling relations from (Vikhlinin et al. 2009a) iteratively to estimate R_{500}, which is then used to measure $T_{\rm x}$, M_g, and M_{500}. Specifically to estimate M_{500}, we use the scaling relation with $Y_{\rm x} = M_g \times T_{\rm x}$

$$M_{500} = (5.77 \pm 0.20) \times 10^{14} h^{0.5} M_\odot \times \left(\frac{Y_{\rm x}}{3 \times 10^{14} M_\odot} \right)^{0.57 \pm 0.03} E(z)^{-2/5}.$$

$Y_{\rm x}$ is chosen as a mass proxy because of its low scatter and insensitivity to the dynamical state of the cluster (Kravtsov et al. 2006; Marrone et al. 2009). More details about the method to estimate M_{500} can be found in Andersson et al. (2011).

In addition to mass, we measure the total X-ray luminosity of each cluster. We first extract an X-ray spectrum of all emission within R500, centered on the X-ray peak, and then we fit this spectrum using a combination of collisionally-ionized plasma (`APEC`) and Galactic absorption (`PHABS`). This allows us to estimate the unabsorbed X-ray flux, which we then convert to a rest-frame luminosity given the known redshift.

6. RESULTS

From Fig. 12, we identify 11 cluster candidates by selecting all objects above the solid blue line, which is the richness limit derived in Section 4.4. The objects below this line are not necessary all isolated AGNs. They may belong to less massive clusters that fall below our selection threshold – here we only consider very massive clusters that should have been included in surveys such as REFLEX (Böhringer et al. 2004) and MACS (Ebeling et al. 2001), but were missed due to the presence of an atypical central galaxy.

Using the NED[13] catalog, we search for known clusters within a 3′ radius of the 11 candidates and report, when available, the redshift of known clusters. In Table 2, we

[13] https://ned.ipac.caltech.edu

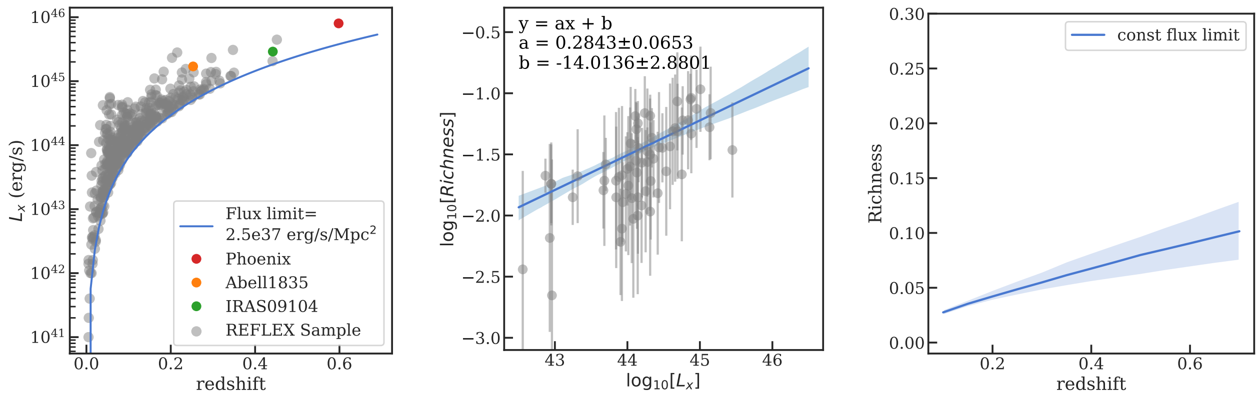

FIG. 11.— Left: the luminosity vs redshift plot for all of the REFLEX clusters with SDSS data. The plot demonstrates the flux-limited nature of the REFLEX survey. The blue line shows the flux limit $= 2.5 \times 10^{37}$ erg/s/Mpc^2. The colored dots show three well-known clusters that should have been detected with the ROSAT catalog. Middle: A plot shows a linear relationship between the luminosity from REFLEX clusters and the measured richness from this work. Right: Richness vs redshift plot with constant flux limit. This plot implies that the REFLEX clusters survey will detect clusters with richness above this constant-flux line.

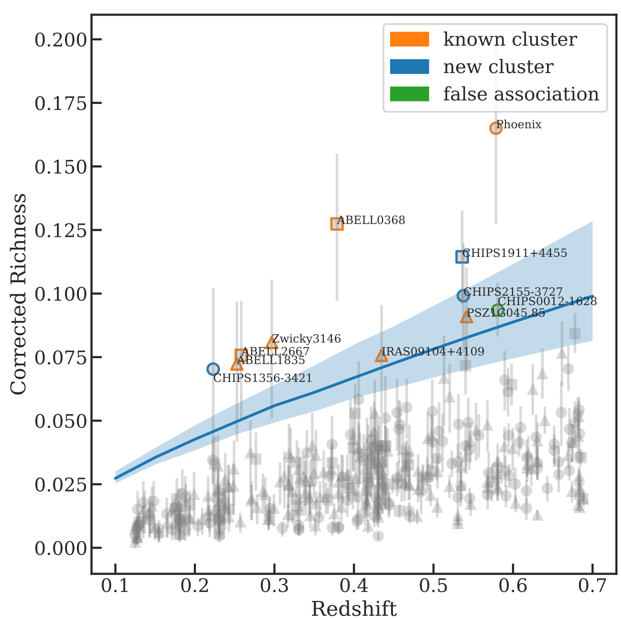

FIG. 12.— Corrected richness versus redshift for all *CHiPS* objects which we follow up in the optical. The blue solid line shows the richness cutoff we used for the survey. It is the same line as the right panel of Fig. 11. Each object is indicated with either a circle, a square, or a triangle based on its optical follow-up telescopes, which are the Magellan telescope (PISCO), Pan-STARRS, or SDSS, respectively. The orange color indicates known clusters above the richness limit while the blue color indicates new cluster candidates with newly-obtained *Chandra* follow-up and the green color indicates false association.

present all 11 candidates with their celestial coordinates, richness, measured redshifts, instruments used to detect, and known clusters associated with each system.

6.1. *Known Clusters Rediscovered*

We find 7 of 11 cluster candidates to be well-known clusters via the NASA Extragalactic Database[14]. In general, these clusters can be divided into two classes: starburst-hosting clusters, such as Abell 1835 (SFR $\sim 100-180\,\mathrm{M_\odot\,yr^{-1}}$; McNamara et al. 2006) and Zwicky 3146 (SFR $\sim 70\,\mathrm{M_\odot\,yr^{-1}}$; Edge et al. 1994), or AGN-hosting clusters, such as Abell 2667 (Rizza et al. 1998) and IRAS 09104+4109 (Crawford & Vanderriest 1996). Another notable example is the Phoenix cluster (McDonald et al. 2012), which has both a starburst-hosting galaxy and a central AGN.

The list of "rediscovered" clusters include some of the most interesting and well-known galaxy clusters in the nearby Universe. It is an interesting question to ask whether they would have been misidentified by ROSAT as isolated point sources had Abell and Zwicky not performed their optical surveys first. At higher redshift and lower mass, where future surveys like *eROSITA* will probe, this issue will likely be exacerbated, requiring multi-wavelength surveys combining X-ray and, for example, optical or SZ, to fully identify the rich variety of galaxy clusters.

6.2. *False Associations*

Only one of the 11 cluster candidates are likely not a galaxy cluster, CHIPS0012-1628. From the NASA Extragalactic Database, a well-known galaxy cluster, Abell 11, is located 2.5' (390 kpc at the redshift of Abell 11) away from the X-ray, mid-IR, and radio bright source that constitutes the center of CHIPS0012-1628. This cluster is close enough that it will boost the number density of galaxies around CHIPS0012-1628. This is not a case where the cluster harbors an extremely active central galaxy but, rather, the superposition of an active galaxy and a rich cluster along the line of sight. As such, we will not perform additional follow-up on this object, and we will exclude it from our catalog.

6.3. *New Cluster Candidates*

The removal of previously-known clusters and false associations leaves us with a sample of three cluster candidates, all of which are rich enough that they should have been detected by ROSAT. Fig. 13 shows optical images of all three candidates, including CHIPS1356-3421,

[14] https://ned.ipac.caltech.edu

TABLE 2
Galaxy cluster candidates/known above the REFLEX flux-limit line in the *CHiPS* Survey

CHiPS Name	RA	DEC	Richness	z[a]	Instruments[b]	Known Cluster	Redshift	Sep (arcmin)
CHIPS2344-4243	356.18375	-42.72208	0.1650	0.5786	PISCO	Phoenix	0.596	0.388
CHIPS0237-2630	39.365	-26.5075	0.1274	0.3787	Pan-STARR	ABELL0368	0.22	0.395
CHIPS1911+4455	287.75415	44.92222	0.1144	0.5361	Pan-STARR	...	0.48	...
CHIPS2155-3727	328.82791	-37.46361	0.0992	0.5376	PISCO	...	...	...
CHIPS0012-1628	3.145	-16.46931	0.0935	0.5807	PISCO	...	...	...
CHIPS1518+2927	229.58292	29.45889	0.0909	0.5416	SDSS	PSZ1G045.85	0.611	0.197
CHIPS1023+0411	155.91374	4.18819	0.0807	0.2966	SDSS	Zwicky3146	0.2805	0.145
CHIPS2351-2605	357.91959	-26.08403	0.0757	0.2583	Pan-STARR	ABELL2667	0.23	0.025
CHIPS0913+4056	138.44167	40.93903	0.0757	0.4347	SDSS	IRAS09104+4109	0.442	0.11
CHIPS1401+0252	210.25876	2.88042	0.0723	0.2528	SDSS	ABELL1835	0.2532	0.055
CHIPS1356-3421	209.023	-34.3531	0.0717	0.2230	PISCO	...	0.223	...

[a] These redshifts are photometric redshfits, estimated in Section 4.1. We picked a peak of the richness histogram as a cluster redshift.
[b] PISCO is the imaging instruments on the Magellan telescope in Chile while SDSS and Pan-STARRS are all-sky optical surveys.

TABLE 3
CHiPS cluster candidates with *Chandra* follow-up

CHiPS Name	z[a]	R_{500} (kpc)	M_{500} ($10^{14}\,M_\odot$)	L_x[b] (10^{44} erg/s)
CHIPS1356-3421	0.223	1300 ± 200	6.4 ± 3.4	5.9
CHIPS1911+4455	0.485	1075 ± 60	6.0 ± 0.1	19
CHIPS2155-3727	~0.5	< 590	< 1	< 1.1

[a] The redshift is measured spectroscopically for the first two objects while the last one only have photometric redshifts used for identifying clusters.
[b] L_x is measured from 0.1-2.4 keV with 1 Mpc aperture.

CHIPS1911+4455, and CHIPS2155-3727. The optical images clearly show an overdensity of red galaxies at the location of the X-ray point source, which is at the center of each field. The three candidates look similar to the Phoenix cluster in that their BCG colors are different from other red member galaxies, implying an active central galaxy.

We followed up all three candidates with new *Chandra* observations over the past two years to search for extended ICM emission, which would confirm the presence of a massive cluster. The optical detection of an overdensity of red galaxies alone usually does not provide enough evidence to claim new galaxy clusters because the line of sight alignment from sheets and filaments of galaxies can coincidentally increase the numbers of red galaxies on the plane of the sky.

Fig 14 shows adaptively-smoothed *Chandra* X-ray images of all three candidates. The rightmost panel of the figure shows that CHIPS2155-3727 has no (or extremely faint) extended X-ray emission, implying that the overdensity of red galaxies we saw in the optical image in Fig 13 is likely a projection effect. The other two panels show extended emissions around bright point sources in the cores. In Table 3, we provide a summary of the X-ray properties (R_{500}, M_{500}, and L_x) for the three cluster candidates, derived from the X-ray images. The first two objects are confirmed massive galaxy clusters with the total cluster mass greater than $3\times10^{14}\,M_\odot$. With our current dataset, we can only provide upper limits for the mass and total luminosity of a cluster for CHIPS2155-3727. In the follow subsections, we discuss each of these three systems in further detail.

6.3.1. *CHIPS1356-3421*

The galaxy cluster surrounding PKS1353-341, also known as CHIPS1356-3421, was the first newly discovered and confirmed galaxy cluster from the *CHiPS* survey with *Chandra* X-ray observations (Somboonpanyakul et al. 2018). It was missed from other X-ray surveys because of an extremely bright AGN in the central galaxy. Apart from the central QSO, the cluster is an ordinary cool-core cluster with $M_{500} = 6.9^{+4.3}_{-2.6} \times 10^{14} M_\odot$ and $L_\mathrm{x} = 7 \times 10^{44}\,\mathrm{erg\,s^{-1}}$ at $z = 0.223$. This cluster, the lowest redshift of the three new *CHiPS* clusters, demonstrates how even massive, nearby clusters can be missed if they harbor central X-ray-bright AGN. We measure a star formation rate (SFR), based on archival UV data, in the central galaxy of CHIPS1356-3421, which is roughly a few percent of the cooling rate − typical of a well-regulated cool core cluster. Given this low star formation rate, we expect that the mid-IR flux is dominated by the central AGN and not by a starburst. More details about this object can be found in our previously published paper (Somboonpanyakul et al. 2018).

6.3.2. *CHIPS1911+4455*

CHIPS1911+4455 is the second galaxy cluster we found by the *CHiPS* survey and confirmed with *Chandra* observations. The photometric redshift of the cluster is $z = 0.48$. It is our most exciting candidate so far. The cluster is unique compared to the other newly discovered galaxy clusters because it harbors a very blue galaxy in the center while surrounded by many red smaller galaxies, similar to the Phoenix cluster (McDonald et al. 2012). Based on the *Chandra* data we obtained, the total mass and the total size of the cluster are $M_{500} = 6.0 \pm 0.1 \times 10^{14}\,\mathrm{M_\odot}$ and$R_{500} = 1075^{+54}_{-66}$ kpc, respectively, which is as massive as CHIPS1356-3421 (Somboonpanyakul et al. 2018).

With our newly obtained *Chandra* data, we measure the core entropy at ~10 kpc to be around 10-20 keVcm^2, which is as cool as in the Phoenix cluster. However, despite having a blue massive central galaxy and a strong cool core, the system shows a highly-disturbed morphology on both large (~50 kpc) and small scale (~20 kpc). Possible scenarios for such a morphology include a recent major merger or a powerful AGN outburst (e.g., Calzadilla et al. (2019)). This finding contradicts ev-

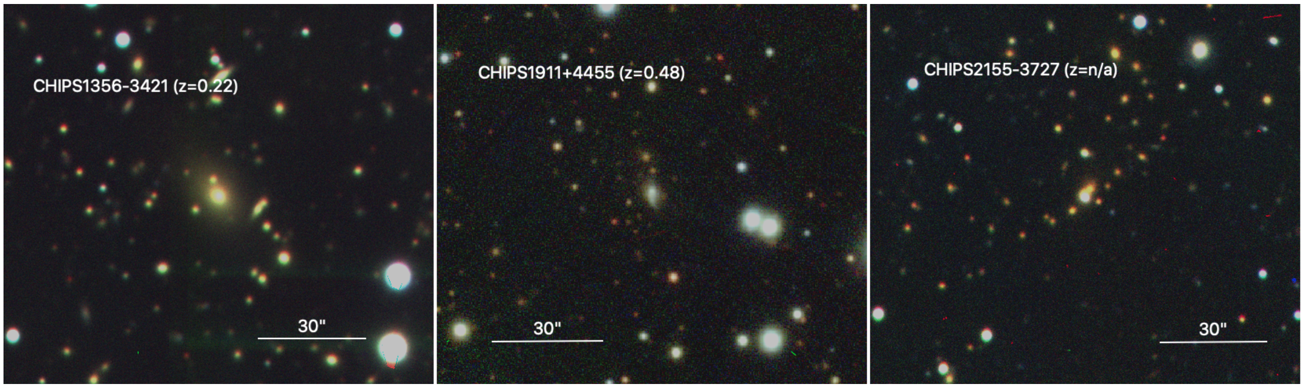

FIG. 13.— This figure shows *gri* optical images of all three candidates, including CHIPS1356-3421, CHIPS1911+4455, and CHIPS2155-3727. These new cluster candidates are visually similar in optical, compared to the Phoenix cluster with extremely bright objects in the center. Based on *Chandra* images, CHIPS2155-3727 appears to not be a massive cluster even though the optical image shows otherwise.

ery other known strong cool core cluster, which are typically highly-relaxed. Additional data will be obtained for this object, including high resolution optical images from the *Hubble* Space Telescope and optical spectra from the Nordic Optical Telescope to look for strong emission lines, a signature of ongoing star formation. A complete analysis of this system is being published in a companion paper, which will include a complete X-ray analysis of the cluster, optical spectroscopy of the central galaxy, and high-resolution Hubble imaging of the cluster core.

6.3.3. *CHIPS2155-3727*

Even though the optical image of CHIPS2155-3727 clearly shows an overdensity of red galaxies at the location of the X-ray source, as shown in Fig. 13, the *Chandra* observation of CHIPS2155-3727 shows no extended emission around the X-ray point source. The non-detection of extended emission in Fig. 14 could imply that the overdensity of galaxies is either a projection of a sheet/filament along the line of sight or a smaller galaxy group below our detection threshold. Spectroscopic data is required to determine whether this is simply a projection effect. Based on the X-ray image, the estimated upper limit for the mass of the cluster, if it exists, is less than $1 \times 10^{14} M_{\odot}$.

7. DISCUSSION

7.1. *Updating Flux-Limited Surveys*

We estimate the rest-frame 0.1-2.4 keV X-ray luminosity, the same as the REFLEX survey, of the new clusters within an aperture of 1 Mpc. Fig. 15 shows the X-ray luminosity of newly discovered galaxy clusters and their redshift with respect to clusters from the REFLEX (Böhringer et al. 2004), eBCS (Ebeling et al. 2000), and MACS (Ebeling et al. 2001) catalogs. These three cluster catalogs were created by first selecting X-ray bright objects from the ROSAT-All Sky Survey and then confirming via an overdensity of galaxies at a common spectroscopic redshift. The solid lines represent the flux limit of the MACS and REFLEX surveys at 1 and $3 \times 10^{-12}\,\mathrm{erg\,s^{-1}\,cm^{-2}}$, respectively. The fact that clusters from these three catalogs follow closely the aforementioned flux limits highlights the clean selection of X-ray surveys, which are biased towards high-mass systems at high-z, but in a mostly predictable way. However, the figure shows that the two *CHiPS* clusters should have been found by these previous X-ray cluster catalogs, which are all based on the ROSAT data, but were not because of their highly-concentrated X-ray profiles. This is, similarly, why the Phoenix cluster was not discovered until recently even though it is the most X-ray luminous clusters known (McDonald et al. 2012).

7.2. *Rarity of Clusters Hosting Extreme Central Galaxies*

One of the main goals of the *CHiPS* survey is to find more galaxy clusters with extreme central galaxies (starbursts and/or AGNs) by looking for clusters around X-ray bright point sources which are also bright in the mid-IR and radio. Given that we have only discovered two new Phoenix-like systems, only one of which has an exceptionally-high star formation rate, we can conclude that such rapidly-cooling systems are extremely rare. From this work, we find that the total number of galaxy clusters with extreme central galaxies to be around 10 objects above the ROSAT detection limit.

To estimate how rare such a system is, we approximate the total population of galaxy clusters found by the ROSAT satellite by combining the REFLEX, eBCS, and MACS samples. Given the total number of clusters detected with the *ROSAT* data to be about 460 in total ($0.1<z<0.7$), the occurrence rate of extreme (starbursts and/or rapidly-accreting AGN) central galaxies is $2 \pm 1\%$. We separate the clusters into two redshift bins to see whether there is any difference. The rate is $2 \pm 1\%$ for nearby objects ($z = 0.1 - 0.3$) while the rate becomes $5 \pm 2\%$ for higher redshift objects ($z = 0.3 - 0.7$). At this stage, we do not see any significant difference between the two redshift bins. A deeper and higher resolution X-ray all-sky survey is required to improve our estimate of the occurrence rate of extreme sources in the center of clusters.

This survey shows that the occurrence rate of clusters hosting extreme central galaxies – defined as systems with either rapidly accreting supermassive black holes or ongoing, massive starburst – is extremely low, of order a few percent. This is consistent with the pink/flicker noise temporal statistics observed in the CCA model and related high-resolution hydrodynamical simulations (Gaspari et al. 2017, 2019), which predict a 2 dex increase

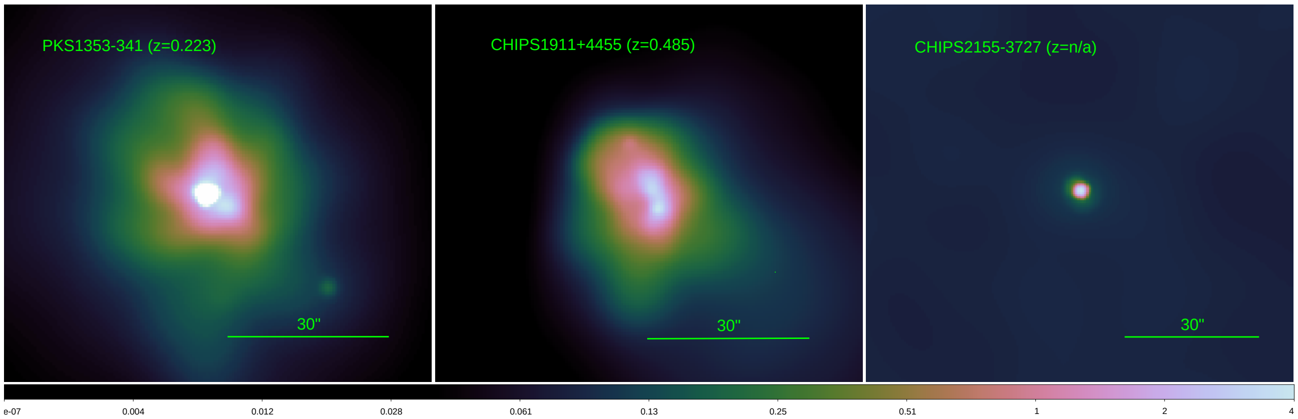

FIG. 14.— The figure shows X-ray images of the three galaxy clusters candidates-CHIPS1356-3421, CHIPS1911+4455, and CHIPS2155-3727. These *Chandra* images confirm the discovery of two new massive galaxies. These two clusters have a relatively bright core, and CHIPS1911+4455 might show a sign of merger. The image of CHIPS2155-3727 only shows a bright point source without any extended emission, meaning that it is unlikely to be a massive cluster.

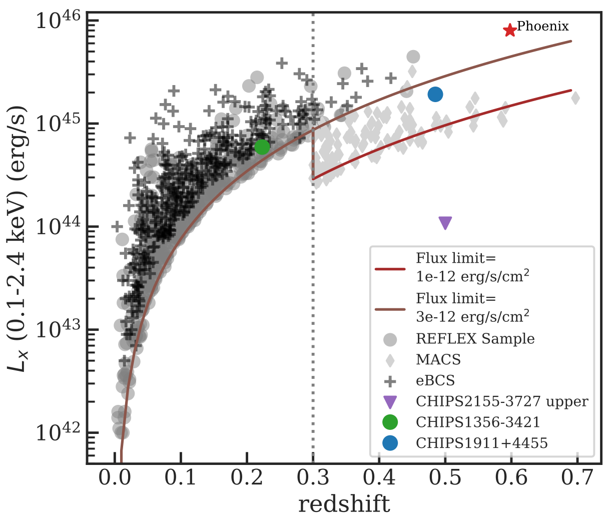

FIG. 15.— Luminosity versus redshift for clusters from the REFLEX Cluster Survey (Böhringer et al. 2004), the ROSAT All-Sky Survey Extended Brightest Cluster Sample (eBCS; Ebeling et al. 2000), and the MAssive Cluster Survey (MACS; Ebeling et al. 2001). The solid lines show X-ray flux limits, introduced by Böhringer et al. (2004), at 1×10^{-12} erg/s/cm^2 and 3×10^{-12} erg/s/cm^2. This figure shows that the Phoenix cluster, CHIPS1356-3421, and CHIPS1911+4455 should have been identified as a cluster by REFLEX, eBCS, and other clusters surveys. The arrow shows an upper limit for CHIPS2155-3727 which shows no detection in our *Chandra* observation.

in the SMBH accretion rate $\sim 1\%$ of the time. Such rarity of quasar-like blast events is in agreement with the tight, gentle self-regulation driven via CCA (arising from the hot halo condensation), which preserves the cool-core structure for several Gyr. Similar rarity is also consistent with the observed scatter in the SFR at fixed cooling rate (Molendi et al. 2016; McDonald et al. 2018), showing 10× higher SFR in less than 10% of clusters.

7.2.1. *Uniqueness of the Phoenix Cluster*

The Phoenix cluster is one of the most unique clusters found recently (McDonald et al. 2012, 2019). The central galaxy of the cluster hosts an extremely X-ray luminous AGN with bright radio jets. High resolution optical/X-ray images also reveal a massive cooling flow extended up to hundreds of kpc, which is accompanied by a starburst-hosting BCG. The estimated star formation rate of its BCG is tremendous at $798 \pm 42\,\mathrm{M_\odot\ yr^{-1}}$ (McDonald et al. 2013), which is the highest of all known clusters. It seems that the AGN feedback, which has been thought to be responsible for stopping the cooling of new stars in central galaxies (Fabian 2012; McNamara & Nulsen 2012), is not effective in the Phoenix cluster, leading to an extremely high star formation rate in the BCG and the presence of a cooling flow. Nonetheless with only one such system, we cannot fully understand where this system fits in our overall understanding of the cooling/feedback cycle. The *CHiPS* survey was designed in part to find more of these systems.

In this work, we find, at most, one potential analog to the Phoenix cluster: CHIPS1911+4455. This system has a high star formation rate ($\sim 100\,\mathrm{M_\odot\ yr^{-1}}$) with complex, filamentary, multiphase gas in the core. Further, based on in-hand Chandra data, we find evidence that the core may be cooling just as rapidly as in the Phoenix cluster (Somboonpanyakul et al. in prep). Considering this, the total number of Phoenix-like clusters are, at most, two (the Phoenix cluster and CHIPS1911+4455) out of $\sim$ 460 systems in a complete X-ray flux-limited sample from the ROSAT-All Sky Survey. This means that the rate of occurrences for such rapidly-cooling systems is around one percent of the massive cluster population. One explanation for such a rare event is that an intense short-lived cooling of the intracluster medium or a short-lived brightening of the central AGN are a part of the AGN feedback cycle and flickering CCA (Gaspari et al. 2011; Prasad et al. 2019). We can roughly estimate how short this burst of cooling would have been if we find only two such systems at $0.1<z<0.7$. Assuming all clusters go through the evolutionary phases in the same manner, within the past ~ 5 Gyr, the rapidly-cooling phase for clusters lasts, on average, for $\sim$22 Myr. Since most signatures of star formation last for roughly 20 Myr (Kennicutt 1998), this implies that almost the fulll cluster population could go through a short-lived phase of rapid cooling, and we would only expect to observe it (and the subsequent young stellar populations) in a few percent of clusters.

7.3. *Planck Cluster Candidates*

Two of the three clusters, CHIPS1356-3421 and CHIPS1911+4455, have corresponding *Planck* cluster candidates at SNR = 5.76 and 4.64, respectively (Planck Collaboration et al. 2016). Specifically, the *Planck* source at the location of CHIPS1356-3421 is among the 1653 SZ detections in the *Planck* catalog, but it is not a member of the 1203 confirmed detections. Somboonpanyakul et al. (2018) shows that it is in fact a massive cool core cluster at that location. Meanwhile, CHIPS1911+4455 has a weaker signal with SNR=4.64 but has an additional counterpart in an external dataset, specifically a significant galaxy overdensity in the WISE data. These two examples show that we could potentially further utilize the *Planck* catalog of unconfirmed SZ sources to help confirm the existence of these hidden clusters with lower richness than what we are able to achieve currently with the *CHiPS* survey.

7.4. *Missing known clusters in the survey*

Based on (McDonald et al. 2018), there are 9 known clusters at $z < 1$ that host a massive star-forming galaxy (SFR > 60 $\mathrm{M_\odot\,yr^{-1}}$) in the center. The *CHiPS* survey rediscovered four of them, including Abell 1835, Zwicky 3146, IRAS 09104+4109, and the Phoenix cluster. The other five are the Perseus cluster, H1821+643, MACS1931.8–2634, RXJ1532.9+3021, and RXJ1504.1–0248. In this section, we explain why these five clusters are not detected in the survey.

The Perseus cluster is the brightest cluster in the X-ray. It is not in our survey because its redshift ($z = 0.0179$) falls outside of our interested range of $0.1 < z < 0.7$. We exclude $z < 0.1$ because there are countless optical surveys looking for massive clusters at that redshift range.

The galaxy cluster surrounding H1821+643 is the only low-redshift ($z = 0.299$) galaxy cluster which contains a highly luminous quasar in the center (Russell et al. 2010). However, the quasar H1821+643 is a radio-quiet quasar (Blundell & Rawlings 2001). It is not included in the *CHiPS* survey because our catalog requires objects to be relatively bright in radio at 1.4 GHz. Furthermore, the *CHiPS* survey is also normalized by the optical images to remove the dependence on redshift; however this also means that we penalize objects which have an extremely bright optical counterpart. These choices were made to reduce the number of candidates to a manageable size for optical follow-up, but will naturally exclude some interesting systems. Thus, we are unable to comment on the occurrence rate of clusters hosting extremely optically-bright or radio-quiet quasars at their center.

MACS1931.8–2634 is another example of a cluster with a powerful AGN outburst amid a major merger event (Ehlert et al. 2011). However, its X-ray location from RASS-BSC and its radio location from NVSS are 36” apart, which is three times larger than our average distance when matching between the two surveys. 1.4 GHz radio observations from the Very Large Array (VLA) shows a brighter Narrow Angle tail (NAT) radio galaxy 45” to the south of the BCG (Ehlert et al. 2011). This radio source could be a power jet from a nearby galaxy that is falling into the BCG. With the 45-arcsecond angular resolution of the NVSS catalog, we conclude that the radio location of MACS1931.8–2634 in NVSS is a blended point between the BCG and the radio galaxy.

The last two clusters, RXJ1504.1–0248 and RXJ1532.9+3021, have relative large star formation rates at $85 \pm 9\,\mathrm{M_\odot\,yr^{-1}}$ and $98 \pm 19\,\mathrm{M_\odot\,yr^{-1}}$, respectively. However, they are not within our mid-IR color-cut for our selection which focuses our selections to the Phoenix cluster. In fact, both of them are very close to our selection cutoff from Section 2. This helps to clarify the baseline type of cluster that we expect to find, specifically clusters with SFR $> 100\,\mathrm{M_\odot\,yr^{-1}}$ in the BCG.

Both 3C 186 and 3C 254 are also not found in the *CHiPS* survey. This is to be expected since the redshfits for both of them are 1.01 and 0.74, respectively, which is more than our redshift cut at 0.7, as mentioned in Section 2.1.

7.5. *eROSITA*

With the recent launch of the extended ROentgen Survey with an Imaging Telescope Array (*eROSITA*) (Predehl et al. 2018) mission in July 2019, an X-ray instrument performing the first imaging all-sky survey in the energy range up to 10 keV, thousands of new galaxy clusters and AGNs will be discovered.

The *CHiPS* survey helps to predict the potential biases in the *eROSITA* survey, if selection is made based solely on the presence of extended X-ray emission. Some massive groups and clusters with extreme BCGs will appear point-like in the X-ray, similar to what we found with the ROSAT all-sky survey and the *CHiPS* survey. Specifically, the types of system that will be missed include systems where the point source dominates the extended emission (e.g., QSO-central clusters) and systems whose cool core appears point-like (e.g., distant, strongly-cooling systems). With the predicted 10^5 clusters found with *eROSITA* (Pillepich et al. 2012), two percent of clusters with extreme central galaxies, as described in Section 7.2, is equal to ~2000 clusters that *eROSITA* will miss if the survey only characterizes extended X-ray emissions as cluster candidates. Pillepich et al. (2012) also estimated that with *eROSITA* cluster counts and cosmology priors from the *Planck* mission, the uncertainty of Ω_m will be less than two percent. Thus, it is crucial to take into account these missing clusters, which appear point-like.

One proposed solution for *eROSITA* is to allow new X-ray detections be classified as both a point source and an extended source if there is any faint extended emission surrounding a point source. This could potentially help identify even more clusters with extreme central properties. Additionally, the upcoming Vera C. Rubin Observatory, a wide-field telescope with 8.4-meter primary mirror, is expected to be operated by 2021 (Ivezić et al. 2019). The telescope will provide an enormous amount of optical data suitable for following up new cluster candidates. An important note for the optical follow-up is the need to allow the presence of non-red BCGs, which is a requirement to many BCG-identifying codes, if we want to find more massive star-forming systems.

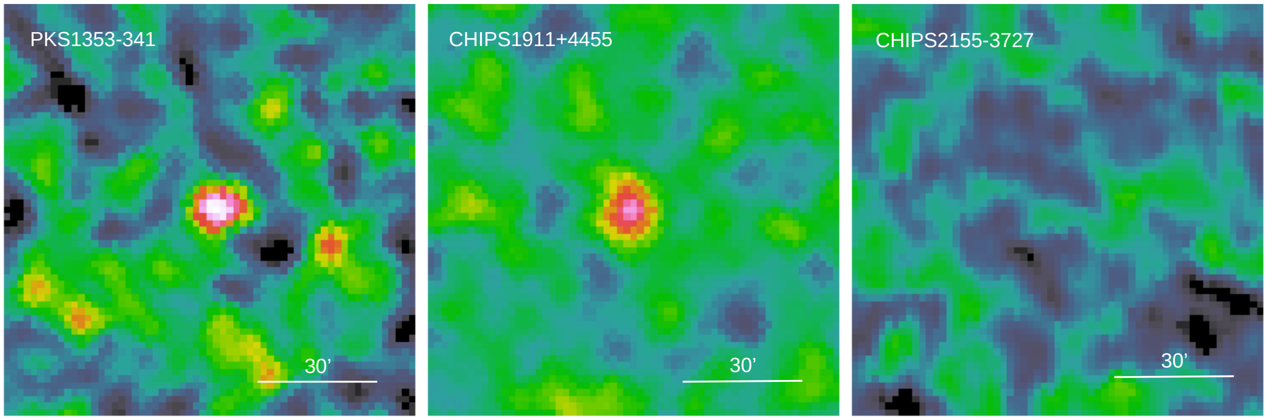

FIG. 16.— This figure shows Y-map images of three galaxy clusters candidates-CHIPS1356-3421, CHIPS1911+4455, and CHIPS2155-3727 (from left to right) from the *Planck* satellite (Planck Collaboration et al. 2016). The two clusters in the left panels are detected with *Planck* and now confirmed with *Chandra*, as described in Section 6.

TABLE 4
LIST OF ALL KNOWN CLUSTERS WITH MASSIVE STAR FORMATION RATE (SFR>60 $M_\odot\,yr^{-1}$)

Cluster Name	z	SFR ($M_\odot\,yr^{-1}$)[a]	CHiPS	Reason not found
RXJ1504.1–0248	0.215	85 ± 9	not found	MIR is outside the range
Abell 1835	0.2528	117 ± 24	found	
Zw3146	0.2966	69 ± 24	found	
IRAS 09104+4109	0.4347	309 ± 120	found	
H1821+643	0.297	447 ± 147	not found	optical is too bright, not radio bright.
Phoenix	0.579	617 ± 200	found	
Perseus	0.0179	71 ± 20	not found	redshift is too low
MACS1931.8–2634	0.352	263 ± 53	not found	no match X-ray vs radio
RXJ1532.9+3021	0.363	98 ± 19	not found	MIR is outside the range

[a] all SFR numbers come from (McDonald et al. 2018).

8. SUMMARY

In this work, we present a complete optical description of the Clusters Hiding in Plain Sight (*CHiPS*) survey, a new galaxy cluster survey using both archival (SDSS and Pan-STARRS) and newly acquired data from the Magellan telescope to find new clusters that harbor extreme central galaxies. Our findings are summarized below:

- By looking at the photometric redshifts of galaxies around X-ray, radio and mid-IR-bright point sources, we have identified 11 cluster candidates. Of these, we rediscovered 7 well-known galaxy clusters with both starburst-hosting and QSO-hosting central galaxies. Three of these candidates have high optical richness coincident with an X-ray source, while the last one fails a secondary inspection. We understand why the last one was misidentified by the automated pipeline which includes projection effects, contamination due to dense star fields near the galactic plane, and contamination from nearby known clusters.

- With additional follow-up data from the *Chandra* X-ray telescope for the three new candidates, we confirmed two newly discovered galaxy clusters. We do not detect extended X-ray emission around the other cluster candidate, finding an upper limit on the total mass of $\sim 10^{14}$ $M_\odot$. Details for the first one, CHIPS1356-3421, or the cluster surrounding PKS1353-341, is already published in our pilot paper (Somboonpanyakul et al. 2018).

- We estimate the total mass and the total luminosity of the other new cluster, CHIPS1911+4455. The total mass (M_{500}), using the $Y_x - M_{500}$ relation, is $6.0 \pm 1.0 \times 10^{14}$ $M_\odot$. Whereas, the X-ray luminosity (0.1-2.4 keV) for this cluster is 1.9×10^{45} erg s^{-1}. This implies that CHIPS1911+4455 is massive enough to be found by previous X-ray clusters surveys, such as the REFLEX and MACS surveys. We also constraint the upper limit for the total mass, CHIPS2155-3727, to be less than 1×10^{14} $M_\odot$.

- We find a massive blue central galaxy with a high star formation rate (120–140 $M_\odot$ yr^{-1}; Somboonpanyakul in prep.) in CHIPS1911+4455, pointing to an extreme central galaxy similar to the Phoenix cluster. With the *Chandra* data, we find the core entropy at $\sim$10 kpc to be as low as in Phoenix, but has a morphology unlike Phoenix and any known strong cool-core cluster. More details about CHIPS1911+4455 will be published in a forthcoming paper.

- With the *CHiPS* survey, we find the occurrence rate of clusters that appear as X-ray point sources with bright mid-IR and radio flux to be $2 \pm 1\%$, and the occurrence rate of clusters with rapidly cooling cores similar to the Phoenix cluster to be $\sim 1\%$. Such rarity is consistent with the flicker-noise statistics expected during the CCA cycles and with its driven average gentle self-regulation.

- One of the primary goals of this survey was to determine if the Phoenix cluster is unique. It looks like it is: there is no clusters at z<0.7 that have a more massive central starburst within factor of ~ 3 in magnitude. If there was, we would have found it in this survey.

In general, the discovery of these CHIPS clusters emphasize a need for X-ray point source/cluster finding algorithms to allow the possibility of finding both point-like and extended objects at the same time. By limiting the algorithm to only pick out X-ray bright point source, many cluster hosting extreme objects (starbursts/AGNs) were missed in the past. These type of objects are critical in our quest to understand the relation between cooling-flow and feedback from the central BCGs. Lastly, by only finding one new galaxy cluster with a massive starburst galaxy in the center (CHIPS1911+4455), we conclude that the Phoenix cluster is in fact a rare occurrence (less than one percent of all the cluster population). This finding will be important in helping us understand the mechanism of forming a Phoenix-like cluster in the future.

Acknowledgments.
Facilities: Magellan-Clay (PISCO, LDSS-3), SDSS, Pan-STARRS, *Chandra X-ray Observatory* (ACIS)
Software: astropy (Astropy Collaboration et al. 2018), CIAO (Fruscione et al. 2006), pandas (McKinney 2010), seaborn (Waskom et al. 2016), confidence interval calculation (Cameron 2011)

T. S. and M. M. acknowledge support from the Kavli Research Investment Fund at MIT, and from NASA through Chandra grant GO5-16143. M. G. is supported by the Lyman Spitzer Jr. Fellowship (Princeton University) and by NASA Chandra GO8-19104X/GO9-20114X and HST GO-15890.020-A grants. A. A. S. and B. S. acknowledge support from NSF grant AST-1814719.

The Pan-STARRS1 Surveys (PS1) and the PS1 public science archive have been made possible through contributions by the Institute for Astronomy, the University of Hawaii, the Pan-STARRS Project Office, the Max-Planck Society and its participating institutes, the Max Planck Institute for Astronomy, Heidelberg and the Max Planck Institute for Extraterrestrial Physics, Garching, The Johns Hopkins University, Durham University, the University of Edinburgh, the Queen's University Belfast, the Harvard-Smithsonian Center for Astrophysics, the Las Cumbres Observatory Global Telescope Network Incorporated, the National Central University of Taiwan, the Space Telescope Science Institute, the National Aeronautics and Space Administration under Grant No. NNX08AR22G issued through the Planetary Science Division of the NASA Science Mission Directorate, the National Science Foundation Grant No. AST-1238877, the University of Maryland, Eotvos Lorand University (ELTE), the Los Alamos National Laboratory, and the Gordon and Betty Moore Foundation.

REFERENCES

Abolfathi, B., Aguado, D. S., Aguilar, G., et al. 2018, ApJS, 235, 42
Allen, S. W., Rapetti, D. A., Schmidt, R. W., et al. 2008, MNRAS, 383, 879
Andersson, K., Benson, B. A., Ade, P. A. R., et al. 2011, ApJ, 738, 48
Astropy Collaboration, Price-Whelan, A. M., Sipőcz, B. M., et al. 2018, AJ, 156, 123
Benítez, N. 2000, ApJ, 536, 571
Bertin, E. 2006, in Astronomical Society of the Pacific Conference Series, Vol. 351, Astronomical Data Analysis Software and Systems XV, ed. C. Gabriel, C. Arviset, D. Ponz, & S. Enrique, 112
Bertin, E. 2011, in Astronomical Society of the Pacific Conference Series, Vol. 442, Astronomical Data Analysis Software and Systems XX, ed. I. N. Evans, A. Accomazzi, D. J. Mink, & A. H. Rots, 435
Bertin, E., & Arnouts, S. 1996, A&AS, 117, 393
Bertin, E., Mellier, Y., Radovich, M., et al. 2002, in Astronomical Society of the Pacific Conference Series, Vol. 281, Astronomical Data Analysis Software and Systems XI, ed. D. A. Bohlender, D. Durand, & T. H. Handley, 228
Bleem, L. E., Stalder, B., Brodwin, M., et al. 2015, ApJS, 216, 20
Bleem, L. E., Bocquet, S., Stalder, B., et al. 2019, arXiv e-prints, arXiv:1910.04121
Blundell, K. M., & Rawlings, S. 2001, ApJ, 562, L5
Böhringer, H., Schuecker, P., Guzzo, L., et al. 2004, A&A, 425, 367
Bouy, H., Bertin, E., Moraux, E., et al. 2013, A&A, 554, A101
Bower, R. G., Benson, A. J., Malbon, R., et al. 2006, MNRAS, 370, 645
Bower, R. G., McCarthy, I. G., & Benson, A. J. 2008, MNRAS, 390, 1399
Calzadilla, M. S., McDonald, M., Bayliss, M., et al. 2019, ApJ, 887, L17
Cameron, E. 2011, PASA, 28, 128
Carlstrom, J. E., Holder, G. P., & Reese, E. D. 2002, ARA&A, 40, 643
Chambers, K. C., Magnier, E. A., Metcalfe, N., et al. 2016, arXiv e-prints, arXiv:1612.05560
Coe, D., Benítez, N., Sánchez, S. F., et al. 2006, AJ, 132, 926
Coleman, G. D., Wu, C. C., & Weedman, D. W. 1980, ApJS, 43, 393
Condon, J. J., Cotton, W. D., Greisen, E. W., et al. 1998, AJ, 115, 1693
Crawford, C. S., & Fabian, A. C. 2003, MNRAS, 339, 1163
Crawford, C. S., & Vanderriest, C. 1996, MNRAS, 283, 1003
Croton, D. J., Springel, V., White, S. D. M., et al. 2006, MNRAS, 365, 11
Dark Energy Survey Collaboration, Abbott, T., Abdalla, F. B., et al. 2016, MNRAS, 460, 1270
Desai, S., Armstrong, R., Mohr, J. J., et al. 2012, ApJ, 757, 83
Donahue, M., Funkhouser, K., Koeppe, D., Frisbie, R. L. S., & Voit, G. M. 2020, ApJ, 889, 121
Ebeling, H., Edge, A. C., Allen, S. W., et al. 2000, MNRAS, 318, 333
Ebeling, H., Edge, A. C., & Henry, J. P. 2001, ApJ, 553, 668
Edge, A. C., Fabian, A. C., Allen, S. W., et al. 1994, MNRAS, 270, L1
Ehlert, S., Allen, S. W., von der Linden, A., et al. 2011, MNRAS, 411, 1641
Fabian, A. C. 2012, ARA&A, 50, 455
Farrow, D. J., Cole, S., Metcalfe, N., et al. 2014, MNRAS, 437, 748
Fruscione, A., McDowell, J. C., Allen, G. E., et al. 2006, Society of Photo-Optical Instrumentation Engineers (SPIE) Conference Series, Vol. 6270, CIAO: Chandra's data analysis system, 62701V
Gaspari, M., Melioli, C., Brighenti, F., & D'Ercole, A. 2011, MNRAS, 411, 349
Gaspari, M., Temi, P., & Brighenti, F. 2017, MNRAS, 466, 677
Gaspari, M., Tombesi, F., & Cappi, M. 2020, Nature Astronomy, 4, 10
Gaspari, M., Eckert, D., Ettori, S., et al. 2019, ApJ, 884, 169
Gladders, M. D., & Yee, H. K. C. 2000, AJ, 120, 2148
Gonzalez, A. H., Gettings, D. P., Brodwin, M., et al. 2019, ApJS, 240, 33
Green, T. S., Edge, A. C., Ebeling, H., et al. 2017, MNRAS, 465, 4872

Gunn, J. E., Siegmund, W. A., Mannery, E. J., et al. 2006, AJ, 131, 2332
Hao, J., McKay, T. A., Koester, B. P., et al. 2010, ApJS, 191, 254
Harrison, C. M. 2017, Nature Astronomy, 1, 0165
Henry, J. P., & Arnaud, K. A. 1991, ApJ, 372, 410
High, F. W., Stubbs, C. W., Rest, A., Stalder, B., & Challis, P. 2009, AJ, 138, 110
High, F. W., Stalder, B., Song, J., et al. 2010, ApJ, 723, 1736
Huchra, J. P., & Geller, M. J. 1982, ApJ, 257, 423
Ivezić, Ž., Kahn, S. M., & Tyson, J. A., e. a. 2019, ApJ, 873, 111
Kelly, P. L., von der Linden, A., Applegate, D. E., et al. 2014, MNRAS, 439, 28
Kennicutt, Jr., R. C. 1998, ARA&A, 36, 189
Kinney, A. L., Calzetti, D., Bohlin, R. C., et al. 1996, ApJ, 467, 38
Kravtsov, A. V., Vikhlinin, A., & Nagai, D. 2006, ApJ, 650, 128
Lang, D., Hogg, D. W., Mierle, K., Blanton, M., & Roweis, S. 2010, AJ, 139, 1782
Lupton, R. H., Gunn, J. E., & Szalay, A. S. 1999, AJ, 118, 1406
Mantz, A. B., von der Linden, A., Allen, S. W., et al. 2015, MNRAS, 446, 2205
Marrone, D. P., Smith, G. P., Richard, J., et al. 2009, ApJ, 701, L114
Mauch, T., Murphy, T., Buttery, H. J., et al. 2003, MNRAS, 342, 1117
McDonald, M., Benson, B., Veilleux, S., Bautz, M. W., & Reichardt, C. L. 2013, ApJ, 765, L37
McDonald, M., Gaspari, M., McNamara, B. R., & Tremblay, G. R. 2018, ApJ, 858, 45
McDonald, M., Bayliss, M., Benson, B. A., et al. 2012, Nature, 488, 349
McDonald, M., McNamara, B. R., van Weeren, R. J., et al. 2015, ApJ, 811, 111
McDonald, M., McNamara, B. R., Voit, G. M., et al. 2019, ApJ, 885, 63
McKinney, W. 2010, in Proceedings of the 9th Python in Science Conference, ed. S. van der Walt & J. Millman, 51
McNamara, B. R., & Nulsen, P. E. J. 2012, New Journal of Physics, 14, 055023
McNamara, B. R., Rafferty, D. A., Bîrzan, L., et al. 2006, ApJ, 648, 164
Mohr, J. J., Armstrong, R., Bertin, E., et al. 2012, in Society of Photo-Optical Instrumentation Engineers (SPIE) Conference Series, Vol. 8451, Proc. SPIE, 84510D
Molendi, S., Tozzi, P., Gaspari, M., et al. 2016, A&A, 595, A123
Motl, P. M., Hallman, E. J., Burns, J. O., & Norman, M. L. 2005, ApJ, 623, L63
O'Sullivan, E., Giacintucci, S., Babul, A., et al. 2012, MNRAS, 424, 2971
Pillepich, A., Porciani, C., & Reiprich, T. H. 2012, Monthly Notices of the Royal Astronomical Society, 422, 44
Planck Collaboration, Ade, P. A. R., Aghanim, N., et al. 2016, A&A, 594, A27
Planck Collaboration, Aghanim, N., Akrami, Y., et al. 2018, arXiv e-prints, arXiv:1807.06209
Prasad, D., Sharma, P., Babul, A., Voit, G. M., & O'Shea, B. W. 2019, arXiv e-prints, arXiv:1909.12888
Predehl, P., Bornemann, W., Bräuninger, H., et al. 2018, in Society of Photo-Optical Instrumentation Engineers (SPIE) Conference Series, Vol. 10699, Proc. SPIE, 106995H
Press, W. H., & Schechter, P. 1974, ApJ, 187, 425
Rizza, E., Burns, J. O., Ledlow, M. J., et al. 1998, MNRAS, 301, 328
Russell, H. R., Fabian, A. C., Sanders, J. S., et al. 2010, MNRAS, 402, 1561
Rykoff, E. S., Rozo, E., Busha, M. T., et al. 2014, ApJ, 785, 104
Schechter, P. 1976, ApJ, 203, 297
Sevilla-Noarbe, I., Hoyle, B., Marchã, M. J., et al. 2018, MNRAS, 481, 5451
Siemiginowska, A., Burke, D. J., Aldcroft, T. L., et al. 2010, ApJ, 722, 102
Siemiginowska, A., Cheung, C. C., LaMassa, S., et al. 2005, ApJ, 632, 110
Skrutskie, M. F., Cutri, R. M., Stiening, R., et al. 2006, AJ, 131, 1163
Somboonpanyakul, T., McDonald, M., Lin, H. W., Stalder, B., & Stark, A. 2018, ApJ, 863, 122
Stalder, B., Stark, A. A., Amato, S. M., et al. 2014, in Proc. SPIE, Vol. 9147, Ground-based and Airborne Instrumentation for Astronomy V, 91473Y
Sunyaev, R. A., & Zeldovich, Y. B. 1972, Comments on Astrophysics and Space Physics, 4, 173
van Dokkum, P. G. 2001, PASP, 113, 1420
Vikhlinin, A., Burenin, R. A., Ebeling, H., et al. 2009a, ApJ, 692, 1033
Vikhlinin, A., Kravtsov, A. V., Burenin, R. A., et al. 2009b, ApJ, 692, 1060
Voges, W., Aschenbach, B., Boller, T., et al. 1999, A&A, 349, 389
Voit, G. M. 2005, Reviews of Modern Physics, 77, 207
Waskom, M., Botvinnik, O., drewokane, et al. 2016, Seaborn: V0.7.1 (June 2016)
Wen, Z. L., & Han, J. L. 2015, MNRAS, 448, 2
Wright, E. L., Eisenhardt, P. R. M., Mainzer, A. K., et al. 2010, AJ, 140, 1868
Yang, L., Tozzi, P., Yu, H., et al. 2018, ApJ, 859, 65